

Fermi surface and pseudogap in electron-doped cuprates

M. M. Zemljčič¹, P. Prelovšek^{1,2} and T. Tohyama³

¹*J. Stefan Institute, SI-1000 Ljubljana, Slovenia*

²*Faculty of Mathematics and Physics, University of Ljubljana, SI-1000 Ljubljana, Slovenia and*

³*Yukawa Institute for Theoretical Physics, Kyoto University, Kyoto 606-8502, Japan*

(Dated: March 23, 2022)

Spectral functions are evaluated numerically within the t - t' - J model as relevant for electron-doped cuprates. The Fermi surface develops from a pocket-like into a large one with doping. The corresponding pseudogap in the nodal direction is well resolved at low doping and vanishes at intermediate doping. Its presence is strongly temperature dependent and thus connected to longer-range antiferromagnetic correlations. Features including double effective band and optical conductivity are consistent with experiments on electron-doped cuprates without invoking the closing of the Mott-Hubbard gap.

PACS numbers: 71.27.+a, 75.20.-g, 74.72.-h

The insight into the interesting and challenging physics of high-temperature superconductors (HTSC) has been greatly enhanced by angle-resolved photoemission spectroscopy (ARPES) experiments on cuprates [1]. One of the challenging aspects is a pronounced asymmetry of spectral properties between more investigated hole-doped and electron-doped cuprates (EDC), as revealed by recent ARPES experiments on representatives of the latter materials, as $\text{Nd}_{2-x}\text{Ce}_x\text{CuO}_4$ (NCCO) [2, 3] and $\text{Sm}_{2-x}\text{Ce}_x\text{CuO}_4$ (SCCO) [4]. While the n-type parent compound Nd_2CuO_4 has very similar excitation spectra to p-type undoped cuprates, the development with doping is different. At low electron doping $x \sim 0.04$ the ARPES Fermi surface (FS) reveals pronounced pockets at $\mathbf{k} = (\pi, 0)$ consistent with doubling of the unit cell due to the long-range antiferromagnetic (AFM) order [2]. With increasing x additional dispersive band-like excitation appears at $\omega < 0$ and reaches the chemical potential ($\omega = 0$) along the diagonal $\mathbf{k} \sim (\pi/2, \pi, 2)$ at intermediate doping $x = 0.15$, which coincides with the disappearance of long-range AFM order and the onset of superconductivity. Consequently, the FS transforms into a large one although still with well resolved quasiparticles only along parts of the FS [2, 3, 4]. More recent analyses of NCCO [3] and SCCO [4] at intermediate doping seem to resolve both effective bands and found the connection with the pseudogap observed in optical conductivity [4, 5]. While in the latter the temperature dependence of the pseudogap reveals relation to the AFM correlations, there is so far no temperature-dependent ARPES data on EDC which would directly relate the ARPES pseudogap to AFM ordering.

On the theoretical side, the EDC represent another very stringent test for microscopic models of HTSC materials. It has become increasingly clear that in prototype Hubbard t - U model and reduced t - J model additional second-neighbor hopping t' (as well as third-neighbor t'') can account well for the asymmetry in several quantities [6, 7]. Still, the origin of the FS transformation from a pocket-like to a large one as found by ARPES remains the central open issue. First theories were based on the strongly renormalized interaction U [8] and the scenario of doping-decreasing U was proposed which results in both Hubbard bands crossing the FS at intermediate

doping [9, 10]. More recent slave-boson approach [11] and numerical calculations within the Hubbard model, using the variation-cluster [12] and dynamical-cluster approaches [13] give indication that most features of FS reconstruction can be reproduced with doping-independent U . More detailed insight into the spectral properties has been obtained from the numerical exact-diagonalization (ED) study of t - t' - t'' - J model at $T = 0$ [7]. However, results show persistence of the pseudogap in the nodal direction even in the overdoped regime. Also, the temperature behavior of the pseudogap in spectral function (SF) has not been clarified yet.

In this Letter we present results of a numerical study of the t - t' - J model at finite $T > 0$ which reveal that most qualitative features of ARPES results are a nontrivial consequence of strong correlations and do not require a doping-dependent model parameters, in particular not the closing of the Mott-Hubbard gap. We show that the pseudogap vanishes with doping in the nodal direction as well as above the pseudogap temperature T^* being closely tied to the disappearance of longer-range AFM correlations. In the same way the FS transforms from a pocket-like into a continuous large one. Further, our results allow for the interpretation of two effective subbands both emerging from an AFM splitting of a correlated (upper Hubbard) band. Numerically evaluated $\sigma(\omega)$ can be also explained within the same pseudogap scenario.

In the following we study the t - t' - J model

$$H = - \sum_{i,j,s} t_{ij} \tilde{c}_{js}^\dagger \tilde{c}_{is} + J \sum_{\langle ij \rangle} (\mathbf{S}_i \cdot \mathbf{S}_j - \frac{1}{4} n_i n_j), \quad (1)$$

where \tilde{c}_{is}^\dagger are projected fermionic operators not allowing the double occupancy of sites. On a square lattice we include besides the nearest-neighbor hopping $t_{ij} = t$ also the second-neighbor hopping $t_{ij} = t'$, where we take $t' = 0.3t$, as relevant for EDC [6, 7]. We also fix $J = 0.3t$.

For the calculation of the SF, $A(\mathbf{k}, \omega)$, we use the finite-temperature Lanczos method (FTLM) [14]. It has been shown that on small systems reachable by ED the calculation at $T > 0$ gives more macroscopic-like results and gives a better controlled approach to $T \rightarrow 0$ provided that $T > T_{fs}$ where

T_{fs} is the finite-size temperature determined by the model and system size [14]. For cases considered here with tilted square lattices of $N = 18, 20$ sites and $N_e = 0 - 4$ doped electrons we have $T_{fs} \sim 0.1 t$. On small systems with fixed boundary conditions one can consider only a discrete set of wavevectors $\mathbf{k}_l, l = 1, N$. To scan the whole Brillouin zone of \mathbf{k} we employ twisted boundary conditions by introducing hopping elements $t_{ij} \rightarrow \tilde{t}_{ij} = t_{ij} \exp(i\vec{\theta} \cdot \vec{r}_{ij})$ in Eq. (1), in this way reaching arbitrary momenta $\mathbf{k} = \mathbf{k}_l + \vec{\theta}$ [7]. Using FTLM we calculate the Green's function $G(\mathbf{k}, \omega)$ and therefrom extract the self energy $\Sigma(\mathbf{k}, \omega) = \omega - \zeta_{\mathbf{k}} - \alpha/G(\mathbf{k}, \omega)$. Borrowing the idea from cluster dynamical mean-field approaches we smoothen $\Sigma(\mathbf{k}, \omega)$ over small interval $\delta k \sim 0.3$ and then recalculate SF. For details we refer to Ref.[16].

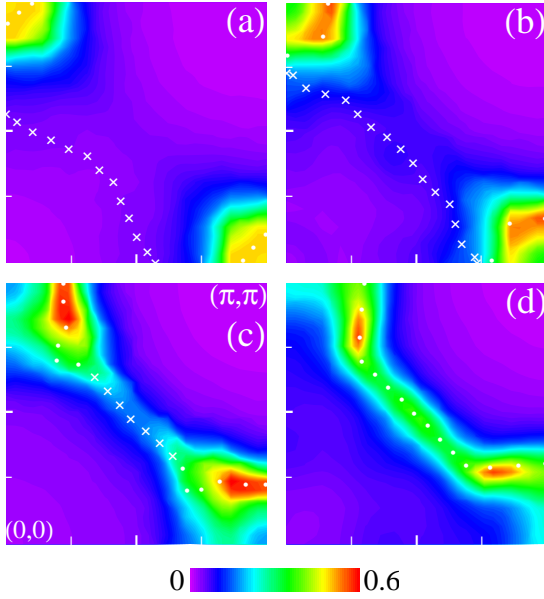


Figure 1: (Color online) Contour plot of $A(\mathbf{k}, \omega = 0)$ representing the Fermi surface for different electron doping: (a) $c_e = 1/20$, (b) $c_e = 2/20$, (c) $c_e = 3/20$, and (d) $c_e = 4/18$. Results are shown for $T/t = 0.1$.

Let us start with the presentation of results for the FS evolution. In Fig. 1 we display the scans of the SF at the chemical potential $A(\mathbf{k}, \omega = 0)$, as usual also in ARPES presentations of FS [1, 2, 3, 4], in the quarter of the first Brillouin zone for different electron dopings $c_e = N_e/N$. Data in Fig. 1 are supplemented with Fig. 2 where full $A(\mathbf{k}, \omega)$ are presented along the AFM zone-boundary line.

At the lowest doping $c_e = 1/20$ in Fig. 1a we get quasiparticle weight forming a circle-like structure around the $(\pi, 0)$ point, well known as the electron pocket consistent with several experimental and theoretical studies [2, 7, 8, 11]. The FS scan looks similar also for $c_e = 2/20$ in Fig. 1b except that the pocket gets more asymmetric weight (opening from the $k_y = 0$ side) around $(\pi, 0)$. Within the rest of the Brillouin zone, in particular along the AFM zone-boundary, the

SF shows a pseudogap at $\omega \sim 0$, as evident also in Figs. 2a,b. In this doping regime the FS can be defined in a usual way, i.e. as a \mathbf{k} -line of points where the quasiparticle peak in SF crosses the chemical potential, represented as white dots around $(\pi, 0)$ in Figs. 1a,b. On the other hand, white crosses in Figs. 1a-c indicate a \mathbf{k} -line where the SF shows symmetric pseudogap. Note that the line of zeroes in the real part of the Green's function determining the Luttinger sum rule is then represented by the combination of both lines. It is indicative in Fig. 1b that already for $c_e = 2/20$ both lines nearly touch as a precursor of a large FS formation.

As the doping is further increased, in Fig. 1c, the FS is formed almost along the whole Luttinger line. The pockets are completely opened and the transfer of the SF weight into the nodal region is observed, although the pseudogap feature remains visible as seen in Fig. 2c. Finally, at $c_e = 4/18$ in Fig. 1d the pseudogap disappears also in the nodal direction resulting in a large continuous FS. In addition, the SF in Fig. 2d are well consistent with the usual quasiparticle peak crossing the chemical potential.

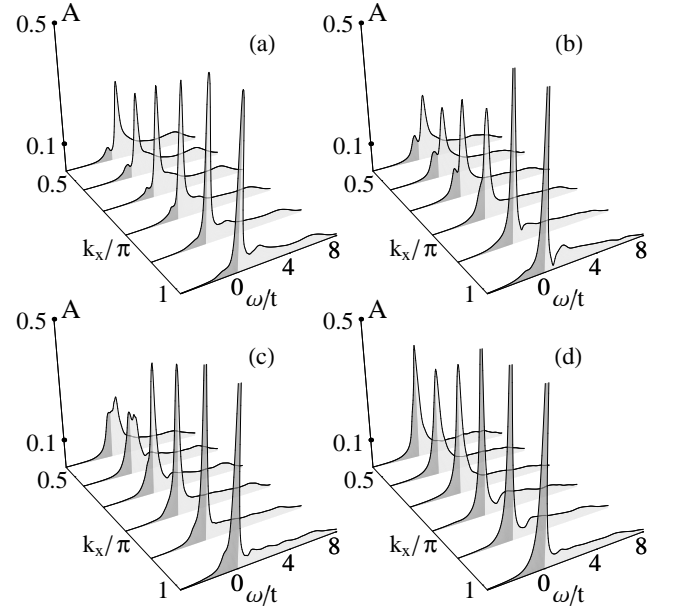


Figure 2: Spectral functions $A(\mathbf{k}, \omega)$ along the AFM zone-boundary line. Dopings are the same as in Fig. 1 and $T/t = 0.1$.

In Fig. 3 we focus in more detail on the doping and temperature dependence of the pseudogap. We present $A(\mathbf{k}, \omega)$ in the nodal point of the Luttinger surface located as shown in the inset of Fig. 3a. It is evident that a pronounced dip in SF at low doping $c_e < 0.15$ fills up with increasing doping and transforms into a usual peak at $c_e = 4/18$. The pseudogap is clearly manifested also in the behavior of the corresponding self-energies $\Sigma''(\mathbf{k}, \omega)$ in Fig. 3b. Besides the overall linear dependence $|\Sigma''(\mathbf{k}, \omega)| \propto \omega$ for $\omega > 0$, characteristic for anomalous (marginal) Fermi liquid and well established also

in hole-doped cuprates [1, 16], additional narrow Lorentzian at $\omega \sim 0$ reveals the pseudogap and its strength [16]. Again, this feature vanishes at $c_e = 4/18$, but as well disappears with increasing T . The intensity (the area) Δ^2 of the pseudogap contribution in $\Sigma''(\mathbf{k}, \omega)$ is the measure of the pseudogap width, i.e. $\propto \Delta$ [16]. Therefore we present in Fig. 3c T -dependence of Δ^2 for different c_e . It is evident that temperature T^* above which the pseudogap effectively disappears decreases with c_e and exists only in the underdoped regime with $c_e < 4/18$. This clearly links pseudogap to the presence of longer-range AFM correlations in the system. In this sense, the pseudogap discussed here is related to large (high-energy) pseudogap observed in hole-doped cuprates [1].

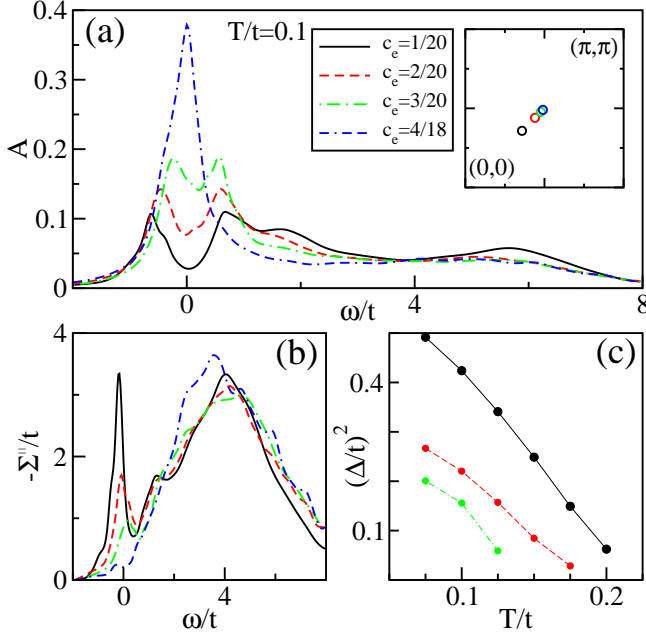


Figure 3: (Color online) a) $A(\mathbf{k}, \omega)$ in the nodal point of the Luttinger surface presented in the inset, b) corresponding self-energies $\Sigma''(\mathbf{k}, \omega)$, and c) pseudogap intensity Δ^2 vs. T for different c_e .

In Fig. 4 we present a weight map of $A(\mathbf{k}, \omega)$ along symmetry lines in the first Brillouin zone. Again, one can notice strong electron-pocket contribution close to $(\pi, 0)$ and evident pseudogap in the nodal direction at lowest $c_e = 1/20$ which becomes less pronounced at higher doping and disappears at $c_e = 4/18$. In addition, it is interesting to follow effective bands which are clearly seen in Fig. 4. At lowest $c_e = 1/20$ one can well resolve the two-band structure, at least along certain \mathbf{k} directions, e.g., along $(0, 0) - (\pi/2, \pi/2)$, $(0, 0) - (\pi, 0)$ as well as $(\pi, 0) - (\pi/2, \pi/2)$. This feature dissolves with doping and finally at $c_e = 4/18$ transforms into a single band. Such a two-band structure is very close to the one observed and analyzed in ARPES on EDC [3, 4]. The weaker band can be interpreted as the shadow-one due to AFM order and its intensity can be linked to AFM order parameter \bar{s} . In fact, results in Fig. 4 can be well represented by effective bands of

the form,

$$\epsilon_{\pm}(\mathbf{k}) = -4\tilde{t}'\gamma'_{\mathbf{k}} \pm \sqrt{(4\tilde{t}\gamma_{\mathbf{k}})^2 + w\bar{s}^2}, \quad (2)$$

where $\gamma_{\mathbf{k}} = (\cos k_x + \cos k_y)/2$, $\gamma'_{\mathbf{k}} = \cos k_x \cos k_y$ are corresponding to first and second-nearest neighbor effective hopping \tilde{t}, \tilde{t}' , respectively. The dispersion of the form (2) can be considered as an effective tight-binding band split due to long-range AFM $\bar{s} \neq 0$ and can be analytically derived from the t - t' - J (or Hubbard) model using the memory-function approach [15] whereby \tilde{t}, \tilde{t}' are renormalized by strong correlations. Very similar bands have been recently used to describe observed ARPES spectra in SCCO [4].

In Fig. 4 we also plot fits of $\epsilon_{\pm}(\mathbf{k})$, with corresponding intensity of subbands shown in the scale from black (no intensity) to white. We note that the main doping dependence emerges through $\bar{s} = 0.35 - 0$ which is the largest for low doping and zero at $c_e = 4/18$ while other parameters are only weakly doping dependent, e.g. $\tilde{t}/t = 0.3 - 0.6$, $-\tilde{t}'/t = 0.1 - 0.2$ and $w = t^2$.

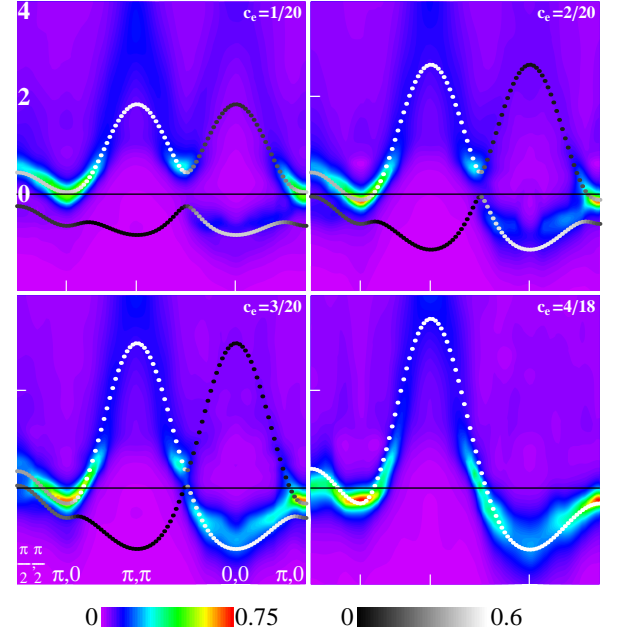


Figure 4: (Color online) Weight map $A(\mathbf{k}, \omega)$ along symmetry lines in the first Brillouin zone for different dopings and $T/t = 0.1$. The fit to split subbands is shown with the corresponding intensities.

Here we comment also on the asymmetry of high-energy dispersion ($\omega < 0$) between hole and electron-doped systems. From Fig. 4 we can clearly see that the dispersion from $(\pi/2, \pi/2)$ to $(0, 0)$ is a rather standard one without significant kinks, but for $\omega > 0$, which corresponds to $\omega < 0$ case of the hole-doped system in $t - t' - J$ models, a kink behavior is seen along $(\pi/2, \pi/2)$ to (π, π) as well as from $(\pi, 0)$ to (π, π) . This difference is consistent with related asymmetry observed in ARPES recently [18]. The details will be given elsewhere [19].

Finally, let us discuss the relation with the optical conductivity $\sigma(\omega)$ in EDC [4, 5] which also shows pronounced pseudogap at low doping. First, we evaluate $\sigma(\omega)$ directly by calculating the dynamical current-current correlations in the ground state at $T = 0$ and via FTLM at $T > 0$ [14, 17]. Results for $T = 0$ and $T/t = 0.15$ at different c_e are presented in Fig. 5. On the other hand, to establish the relation with the pseudogap observed in SF we also consider the simplest (decoupling) approximation in terms of SF neglecting the vertex corrections,

$$\sigma_d(\omega) = \frac{2\pi}{\omega N} \sum_{\mathbf{k}} (v_{\mathbf{k}})^2 \int d\omega' g(\omega, \omega') A(\mathbf{k}, \omega') A(\mathbf{k}, \omega' - \omega), \quad (3)$$

where $g(\omega, \omega') = f(\omega' - \omega) - f(\omega')$ and $v_{\mathbf{k}}$ are bare band velocities as determined by t, t' . Numerically evaluated SF as presented above are inserted into Eq. (3) and results are plotted in Fig. 5 as black lines. A nontrivial message following from Fig. 5 is that $\sigma_d(\omega)$ yields very good overall qualitative and even quantitative agreement with the exactly evaluated $\sigma(\omega)$ (at $T > 0$), whereby features are plausibly broader in $\sigma_d(\omega)$.

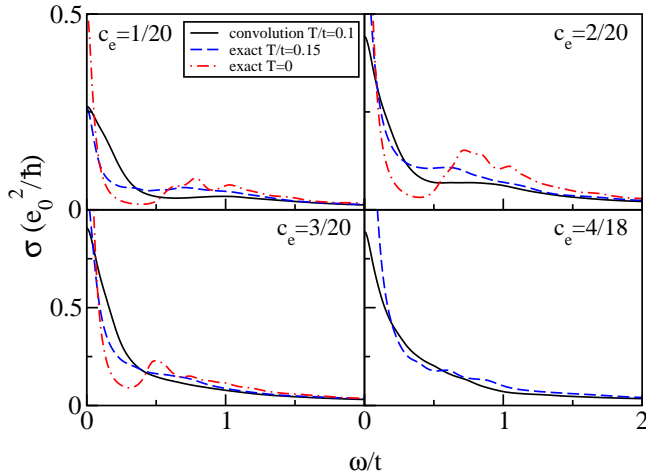


Figure 5: (Color online) Optical conductivity $\sigma(\omega)$ as obtained from the small-system calculation at $T = 0$ (red line), shown for $c_e = 1/20, 2/20, 3/20$, and $T/t = 0.15$ (blue line). Black lines represent $\sigma_d(\omega)$ calculated from the convolution of spectral functions at $T/t = 0.1$.

At low doping, $c_h = 1/20, 2/20$ we can observe at $T/t = 0.15$ a hump in $\sigma(\omega)$ at $\omega/t \sim 0.7$, even more pronounced at $T = 0$, which can be interpreted as a manifestation of the pseudogap. The same peak-dip feature is also resolved (although with somewhat shifted peak) in convoluted $\sigma_d(\omega)$ which is the indication that the pseudogap in conductivity has the same origin as the one in the SF. Furthermore, $v_{\mathbf{k}}$ is the largest along the nodal part of the FS so it is plausible that $\sigma(\omega)$ also tests the nodal pseudogap. Further doping suppresses the peak-dip feature in Fig. 5 at $c_e = 4/18$ which can be related to the simultaneous pseudogap disappearance in $A(\mathbf{k}, \omega)$.

In conclusion, presented results for spectral functions and optical conductivity show overall good qualitative and even quantitative agreement with experimental results on EDC with different doping, both for ARPES on NCCO and SCCO [2, 3, 4], and $\sigma(\omega)$ [4, 5]. Since we have used the simplest prototype model, Eq.(1), for strongly correlated electrons with fixed parameters, observed nontrivial phenomena as the Fermi surface reconstruction, pseudogap and split bands appear as a direct consequence of strong correlations. So there is no need to invoke a doping-dependent Mott-Hubbard gap.

In comparison with more investigated hole-doped cuprates, EDC seem to have an advantage that anomalous SF as well as $\sigma(\omega)$ can be explained in a more straightforward way by invoking the long-range AFM order \bar{s} , persisting in EDC materials up to $c_e = 0.15$. In particular, the double effective bands as seen in Fig. 4 at lower doping as well as in recent ARPES experiments [3, 4] can be interpreted with a band splitting proportional to \bar{s} , Eq.(2), which disappears in the overdoped regime.

The pseudogap which is pronounced in SF along the zone diagonal and in $\sigma(\omega)$, shows strong doping and temperature dependence, whereby we can establish the pseudogap temperature $T^*(c_e)$ consistent with the one deduced from the optical conductivity $\sigma(\omega)$ [5] but so far not analyzed with ARPES. Both doping and T -dependence clearly establish longer-range AFM correlations as the origin of the pseudogap in EDC.

This work was supported by the Slovenian Research Agency under grant PI-0044. T.T. acknowledges supports from the Next Generation Super Computing Project of Nanoscience Program, CREST, and Grant-in-Aid for Scientific Research from MEXT, Japan.

-
- [1] A. Damascelli, Z. Hussain, and Z.-X. Shen, *Rev. Mod. Phys.* **75**, 473 (2003).
 - [2] N. P. Armitage *et al.*, *Phys. Rev. Lett.* **88**, 257001 (2002).
 - [3] H. Matsui *et al.*, *Phys. Rev. Lett.* **94**, 047005 (2005).
 - [4] S. R. Park *et al.*, *Phys. Rev. B* **75**, 060501(R) (2007).
 - [5] Y. Onose, Y. Taguchi, K. Ishizaka, and Y. Tokura, *Phys. Rev. Lett.* **87**, 217001 (2001).
 - [6] T. Tohyama and S. Maekawa, *Phys. Rev. B* **64**, 212505 (2001).
 - [7] T. Tohyama, *Phys. Rev. B* **70**, 174517 (2004).
 - [8] H. Kusunose and T. M. Rice, *Phys. Rev. Lett.* **91**, 186407 (2003).
 - [9] C. Kusko, R. S. Markiewicz, M. Lindroos, and A. Bansil, *Phys. Rev. B* **66**, 140513(R) (2002).
 - [10] D. Senechal and A. -M. S. Tremblay, *Phys. Rev. Lett.* **92**, 126401 (2004).
 - [11] Q. Yuan, F. Yuan, and C. S. Ting, *Phys. Rev. B* **72**, 054504 (2005).
 - [12] M. Aichhorn, E. Arrigoni, M. Potthoff, and W. Hanke, *Phys. Rev. B* **74**, 235117 (2006).
 - [13] A. Macridin, M. Jarrell, Th. Maier, P. R. C. Kent, and E. D'Azevedo *Phys. Rev. Lett.* **97**, 036401 (2006).
 - [14] for a review see J. Jaklič and P. Prelovšek, *Adv. Phys.* **49**, 1 (2000).
 - [15] P. Prelovšek and A. Ramšak, *Phys. Rev. B* **63**, 180506(R) (2001).

- (2001)
- [16] M. M. Zemljich and P. Prelovšek, cond-mat/0608310.
- [17] M. M. Zemljich and P. Prelovšek, Phys. Rev. B **72**, 075108 (2005).
- [18] Z. -H. Pan *et al.*, cond-mat/0610442.
- [19] M. M. Zemljich, P. Prelovšek and T. Tohyama, unpublished.